ASIAN JOURNAL OF CIVIL ENGINEERING (BUILDING AND HOUSING) VOL. 13, NO. 3 (2012)
PAGES 301-318

DETECTION OF A THROUGH-THICKNESS CRACK BASED ON ELASTIC WAVE SCATTERING IN PLATES PART I: FORWARD SOLUTION

N. Khaji* and H. Kazemi Noureini
Faculty of Civil and Environmental Engineering, Tarbiat Modares University, Tehran, Iran

Received: 2 August 2011; **Accepted:** 5 October 2011

ABSTRACT

In the first part of the present paper, a numerical method called spectral finite element method (SFEM) is presented, which is able to simulate wave scattering phenomena in plates. Combining excellent characteristics of classical finite element method (FEM) and spectral elements, SFEM not only exhibits flexibility and ease of formulation, which is a FEM character, but also exploiting high order spectral elements leads to a significant superiority over FEM from the viewpoints of solution precision and computation costs. The excellent characteristic of SFEM is its diagonal mass matrix because of the choice of the Lagrange interpolation function supported on Legendre-Gauss-Lobatto (LGL) points in conjunction with LGL integration rule. Therefore numerical calculations can be significantly efficient in comparison with the classical FEM. In this paper, a SFEM-based code is represented and verified, and then some wave propagation problems in elastic solid domains are solved using this code to show the capabilities of SFEM in solving elastodynamic problems. The problems are solved using different spectral elements, and then solution accuracy and computational costs in different solutions are compared to analytical and/or numerical solutions available in the literature. In the second part of this paper, the result of this part as forward solution is used for detection of through-thickness crack in plates.

Keywords: Spectral finite element method; elastodynamics; wave scattering analysis

1. INTRODUCTION

Elastodynamics covers a broad range of phenomena in engineering and physical problems, in which general form of wave equations with suitable boundary conditions (BCs) should be solved. During the last decades, numerical methods have provided robust and effective forums to challenge wave propagation phenomenon among which, finite difference method (FDM) [1], finite element method (FEM) [2–6], and boundary element method (BEM) [7–15] are most popular.

* E-mail address of the corresponding author: nkhaji@modares.ac.ir (N. Khaji)

High-order methods on the other hand, have attracted high interest in the last years, to improve computational efficiency and reduce computation costs needed for an elastodynamic simulation. Regardless of the method, the approximated solution is described in terms of high-order polynomial basis. High-order methods are always associated with not only high accuracy and computational efficiency but also some well-known drawbacks. For instance, FDM are not very well suited for describing very complex geometries and heterogeneous media. Moreover, boundary conditions are difficult to implement in FDM. Last but not least, classical high-order FEMs are known to generate high-order spurious modes [16].

To overcome these problems, spectral finite element method (SFEM) has been developed. Recently, two different kinds of SFEM have been proposed for analysis of wave propagation, namely, fast Fourier transform (FFT)-based SFEM and orthogonal polynomials-based SFEM. The latter one, which employs orthogonal polynomials, is much more suitable for analyzing wave propagation in domains with complex geometry. SFEM gain the best of both worlds by hybridizing spectral and finite element methods. The domain is subdivided into elements, as in FEs, to gain the flexibility and matrix sparsity of FEs. At the same time, the degree of the polynomial in each sub-domain is sufficiently high to retain the high accuracy and low storage of spectral methods.

When it comes to mention the differences between FEM and SFEM, the major difference is that spectral analysis consists of selection of specific basis functions and the collocation points. Orthogonal basis functions are used as approximation functions and such selection of approximation functions in conjunction with specific numerical integrating schemes used in SFEM, leads to a diagonal mass matrix which is a great advantage over FEM. Fourier series, Chebyshev and Legendre polynomials are the commonly used basis functions. In this research, Legendre polynomials have been chosen as basis functions, and as will be discussed, the roots of the first derivative of a Legendre polynomial of order N would contribute in the collocation points set.

SFEM which was originally introduced in computational fluid mechanics [17] is currently being implemented in continuum-based elastodynamics problems [18–21]. More recently, the SFEM was used to simulate wave propagation in both sound and damaged structures. For example, wave propagation in one-dimensional (1D) structures, such as rod and beam, were investigated by Sridhar *et al.* [16] and Kudela *et al.* [22]. Sridhar *et al.* [16] also presented various comparisons between situations where FEs and SFEs were used to solve the same problems and it was brought out that SFEM is significantly more efficient than classical FEM from the viewpoints of time and memory costs. Results of numerical simulation of the transverse elastic wave propagation in a composite plate were presented by Kudela *et al.* [23]. A two-dimensional (2D) spectral membrane finite element-based model was developed by Zak *et al.* [24], and was used for the analysis of wave propagation in a cracked isotropic panel.

As SFEM has shown a promising performance in solving problems in which elastic wave propagation plays an important role, the aim of the present paper is to show how this method could be formulated and coded in the most efficient way to simulate wave scattering phenomena in plates, with less computational effort while obtaining the highest resolution. As illustrated in the second part of this paper, a solution of wave scattering phenomena of highest resolution play a critical role as forward solution for detection of through-thickness crack in plates.

2. FORMULATION OF 2D SPECTRAL FINITE ELEMENTS

The following presentation is assumed for isotropic, homogeneous, and small-displacement linear elastic behavior of materials. The Legendre polynomials-based 2D spectral finite element (SFE) discretization proceeds as what follows. The domain W is firstly decomposed into a number of non-overlapping quadrilaterals, W_e, as in classical FEM. These elements are subsequently mapped into a reference domain $L=[-1,1]^2$, a square in 2D, using an invertible local mapping *f*. On the reference domain L, a set of basis functions consisting of Legendre polynomials of degree, n_l, are introduced. Subsequently, a set of nodes are defined (denoted by $x_i \in [-1,1]$, $i=1,2,\mathbf{K},n_l+1$) which are the Legendre-Gauss-Lobatto (LGL) points. The LGL points are the (n_l+1) roots of

$$(1-x^2)\,L'_{n_l}(x)=0 \tag{1}$$

where $L'_{n_l}(x)$ is the first derivative of the Legendre polynomial of order n_l. The definition of element nodes results in an irregular distribution of nodes, as shown in Figure 1, which is different from classical FEs with uniformly spaced nodes within elements or on the element boundaries.

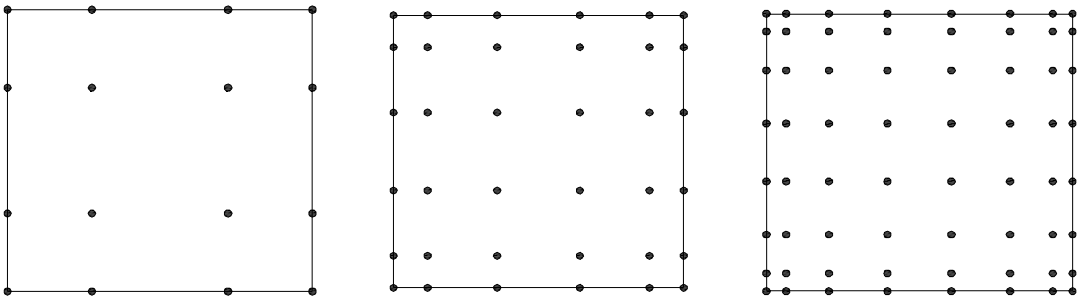

(a) (b) (c)

Figure 1. Various spectral elements with a certain degree of Lagrange polynomials: (a) $n_l=3$, (b) $n_l=5$, (c) $n_l=7$

Any quantity such as *f* may be interpolated on element's domain using the following relation

$$f\left(x(x,h)\right)=\sum_{n=1}^{n_n} N_n(x,h)\,f_n=\sum_{i=1}^{n_l+1}\sum_{j=1}^{n_l+1} h_n^{n_l}(x)h_n^{n_l}(h)\,f_{ij} \tag{2}$$

where n_n indicates the total number of nodes in one spectral element, and f_{ij} is the value of interpolated quantity *f* at collocation point (x_i,h_j)

$$f_{ij} = f\left(x(x_i, h_j)\right) \tag{3}$$

and $N_n(x,h)$ is the nth node's shape function as

$$N_n(x,h) = h_n^{n_l}(x) h_n^{n_l}(h) \tag{4}$$

in which $h_n^{n_l}(x)$ and $h_n^{n_l}(h)$ denote the nth node's shape functions in x and h natural coordinates directions, respectively. Moreover, the LGL shape functions used in this research are in the following form

$$h_n^{n_l}(\xi) = \frac{(\xi-\xi_1)(\xi-\xi_2)\,\mathbf{L}\,(\xi-\xi_{n-1})(\xi-\xi_{n+1})\,\mathbf{L}\,(\xi-\xi_{n_l+1})}{(\xi_n-\xi_1)(\xi_n-\xi_2)\,\mathbf{L}\,(\xi_n-\xi_{n-1})(\xi_n-\xi_{n+1})\,\mathbf{L}\,(\xi_n-\xi_{n_l+1})} \tag{5}$$

In an elastodynamic problem, the dynamic equilibrium equations (6) should be satisfied during the time of analysis [20]

$$[M]\ddot{\mathbf{u}} + [C]\dot{\mathbf{u}} + [K]\mathbf{u} = \mathbf{F} \;,\; \mathbf{F} = -\mathbf{F}_t - \mathbf{F}_{ext} \tag{6}$$

where $[M]$, $[C]$, and $[K]$ are the global mass, damping, and stiffness matrices, respectively. In addition, $\mathbf{F}_t$ and $\mathbf{F}_{ext}$ are the discrete representations of forcing terms for external traction and body force, respectively. In a wave propagation analysis, the damping term of the system of equations, $[C]\dot{\mathbf{u}}$, could be neglected [25]. Thus, the dynamic equilibrium equations could be written in the form of Equation (7)

$$[M]\ddot{\mathbf{u}} + [K]\mathbf{u} + \mathbf{F}_t + \mathbf{F}_{ext} = \mathbf{0}, \tag{7}$$

in which global mass and stiffness matrices may be represented in the following forms

$$[M] = \sum_{e=1}^{n_e} [M^e] \;,\; [K] = \sum_{e=1}^{n_e} [K^e] \tag{8}$$

and load vectors are

$$\mathbf{F}_t = \sum_{e=1}^{n_e} \mathbf{F}_t^e \;,\; \mathbf{F}_{ext} = \sum_{e=1}^{n_e} \mathbf{F}_{ext}^e \tag{9}$$

where $[M^e]$, $[K^e]$, $\mathbf{F}_t^e$, and $\mathbf{F}_{ext}^e$ respectively have the same definitions as global variables $[M]$, $[K]$, $\mathbf{F}_t$, and $\mathbf{F}_{ext}$, at the element level *e*. Elemental mass and stiffness matrices may be written as

$$[M^e]=\int_{W_e} r[N]^T[N]dW_e \quad , \quad [K^e]=\int_{W_e}[B]^T[C][B]dW_e \tag{10}$$

Furthermore, the load vectors could be represented as

$$\vec{F}_t^e=-\int_{G_e}[N]^T\vec{t}\,dG_e \quad , \quad \vec{F}_{ext}^e=-\int_{W_e}[N]^T\vec{f}\,dW_e \tag{11}$$

The above integrals should be integrated using LGL numerical integrating scheme which uses spectral collocation points as sampling points. Each collocation point is associated with a spectral integrating weight represented by

$$w_{x_i}=\frac{2}{n_l(n_l+1)\left(L_{n_l}(x_i)\right)^2} \quad , \quad i=1,2,\mathbf{K},n_l+1 \tag{12}$$

where L_{n_l} is the Legendre polynomial of order n_l.

The second-order ordinary differential equation (7) may be solved using central difference time integration scheme, which is conditionally stable. When $\Delta t \le \Delta t_{cr} \cong \frac{L_{\min}}{c}$, the central difference time integration scheme is stable, where $L_{\min}$ is the minimum distance between two adjacent nodes and c is the wave velocity in elastic medium. While using central difference time integration scheme, the global stiffness matrix does not need to be actually assembled [25]. Therefore, the required computations could be performed on the elemental level. Another major point of this scheme is that as the order of SFEs increases, the minimum distance between SFEs' nodes decreases very fast. In other words, the critical time increment is significantly decreased, so there should be a balance between the mesh size and the order of SFEs to avoid unnecessary growth in computation time. More details in this regard may be found in [20].

3. NUMERICAL EXAMPLES

The above methodology has been implemented in a 2D time-domain SFEM code. In this code written in FORTRAN environment, a library of spectral quadrilateral elements with various orders is provided. In this research, GID as a freeware for pre-processing purposes is linked to the SFEM code (see Figure 2). Furthermore, TECPLOT is used to show the results of analyses in post-processing steps. The detailed flow-chart of the developed software using FORTRAN code, GID, and TECPLOT may be observed in Figure 3.

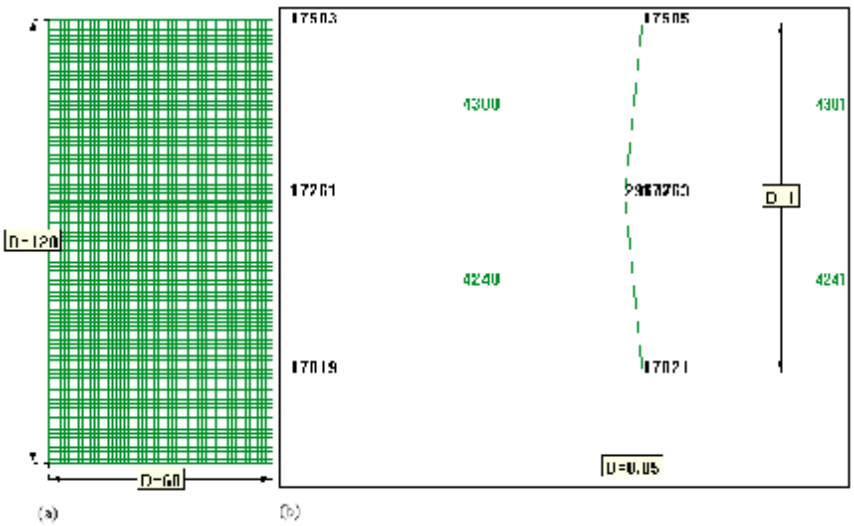

Figure 2. A sample mesh shown using GID: (a) rectangular domain with an embedded crack, (b) detailed view of cracked zone

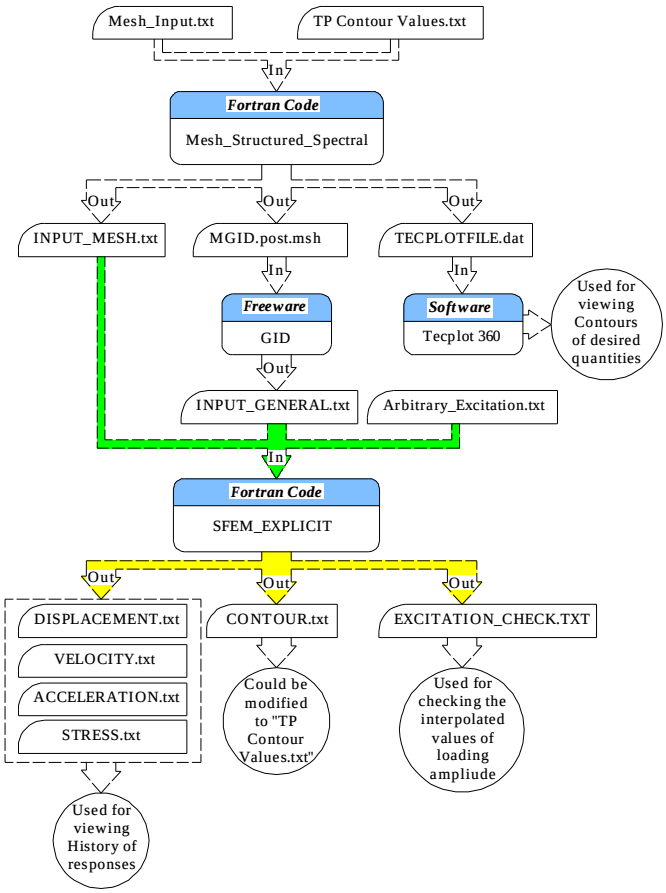

Figure 3. The detailed flow-chart of the developed SFEM software

In order to validate the nature and general behavior of the developed software, three numerical examples are considered. A plane stress condition is assumed for all the examples. Numerical results are compared with those obtained by exact analytical solutions [26] and/or by classical FEM to assess the stability and the accuracy of the present method. No physical damping (i.e., pure elastic material behavior) is considered in all the SFEM analyses. All quantities are measured in SI units.

3.1 Rectangular bar subjected to heaviside loading

In the first example, verification of the developed software especially in comparison with analytical solutions is the main target. A rectangular bar (see Figure 4a), whose length *L* is twice its width *W*, is fixed at its left end with traction free on its top and bottom sides. The Poisson's ratio is considered zero to impose 1D condition. The right end side of bar is uniformly subjected to a Heaviside step function representing a suddenly applied load ($P_0 = 1$) as shown in Figure 4b. The material constants are as follows: the Young's modulus $E = 1$, and the mass density $r = 1$. These material properties yield the maximum propagation velocity of stress waves $c = 1$. To show the convergence of the SEM, two different meshes are used and the results are compared to the analytical solutions. Each mesh includes only two square elements with a specific degree of Lagrange polynomials. The first mesh is constructed using 36-nodes elements and the second mesh uses 441-nodes elements. In fact, the second mesh may represent an extreme of SFEM precision.

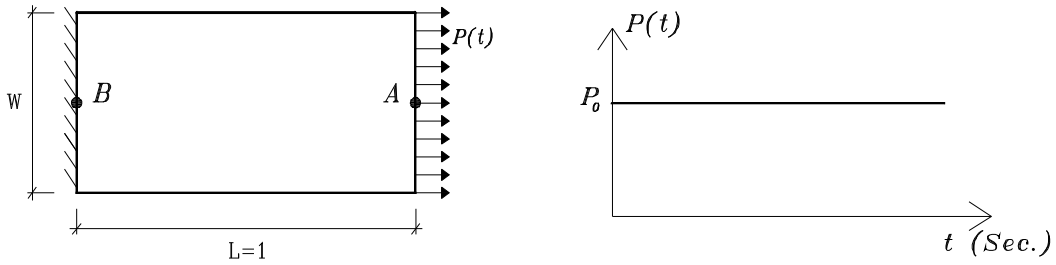

(a) (b)

Figure 4. The first example. Rectangular bar subjected to prescribed loading: (a) geometry and boundary conditions, (b) Heaviside loading

The time histories of horizontal displacement at point A and horizontal stress at point B (see Figure 4a) are investigated. The numerical results by SFEM are compared with those of analytical solution. Figure 5 depicts the horizontal displacement of point A, for the Heaviside step function loading. As it is obvious from this figure, both types of spectral elements give very good results and that the higher-order elements give the better results.

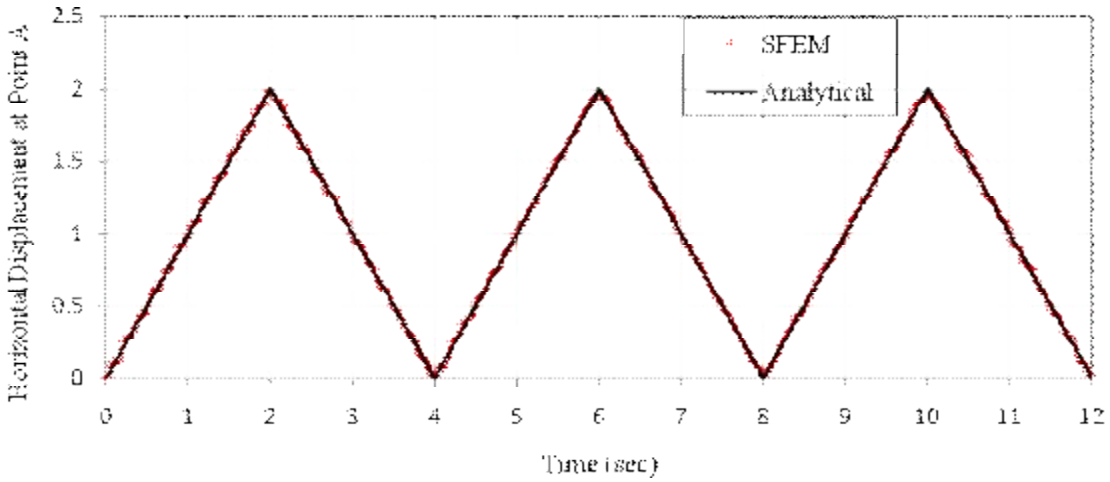

(a)

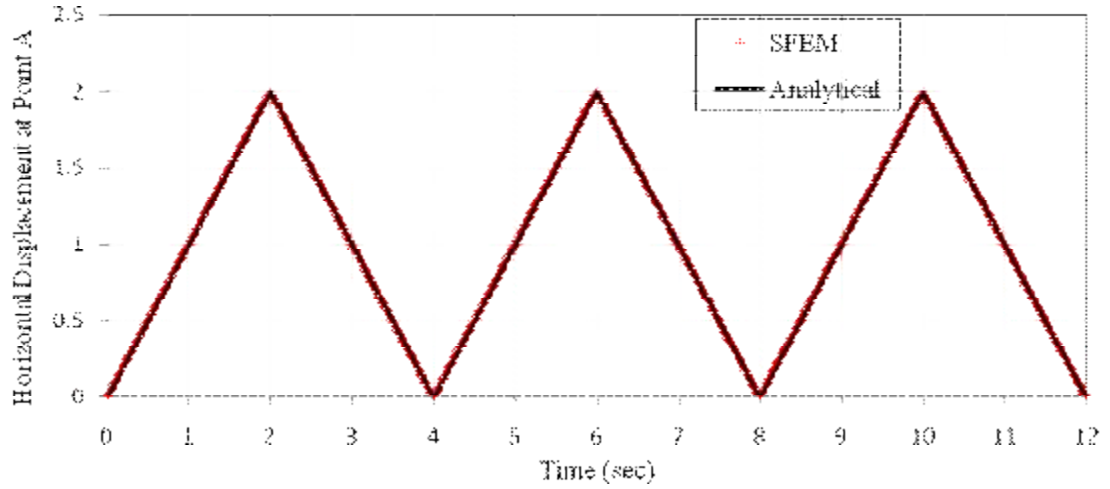

(b)

Figure 5. Horizontal displacement at point A due to the Heaviside loading, (a) 36-nodes elements, (b) 441-nodes elements

The horizontal stress histories at point B, for the Heaviside step function loading is shown in Figure 6. Good agreement between the SFEM results and the analytical solution can be observed, especially with higher-order elements. The SFEM results experience small oscillations around the analytical solutions at moments when the stress jumps. This type of oscillations are caused by the sudden application of the step load, and also observed in other numerical studies such as boundary element method (BEM) [7], domain boundary element method (D-BEM) [10], and hybrid BEM-FEM approach [27,28].

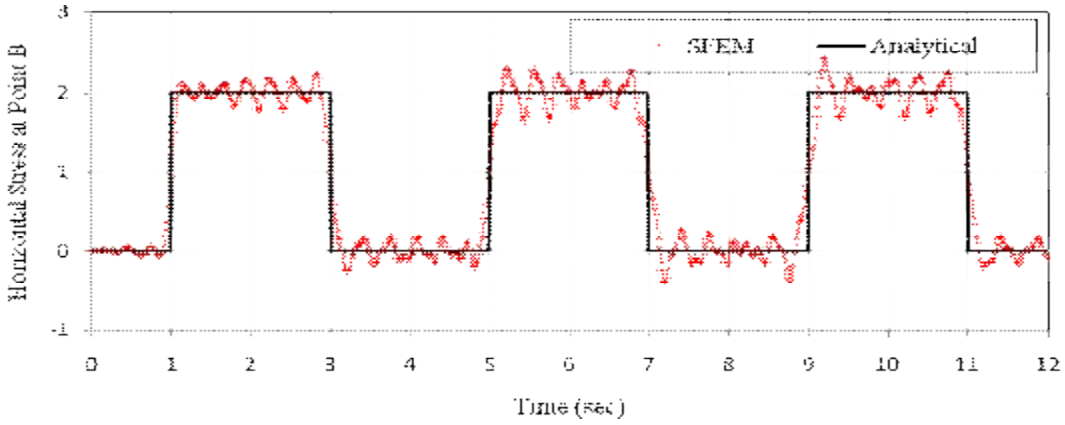

(a)

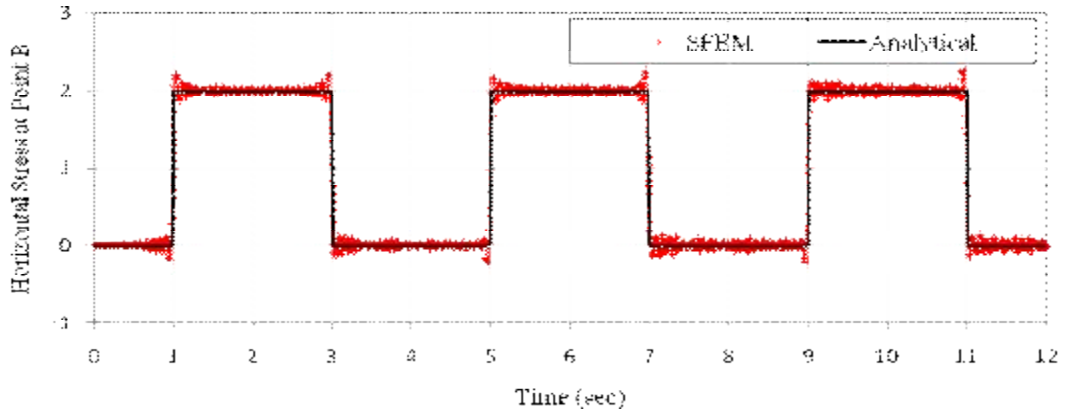

(b)

Figure 6. Horizontal stress at point B due to the Heaviside loading, (a) 36-nodes elements, (b) 441-nodes elements

As it is shown in Figure 6, the horizontal stress at point B obtained using 441-nodes ($n_l+1=21$) elements is much more accurate than that of 36-nodes ($n_l+1=6$) elements. However, it should be noted that as mentioned previously, employing such high-order elements causes Δt_{cr} to decrease rapidly and thus the computations require much more time. In this case, a $\Delta t=0.01\,\text{sec}$ was used for the first analysis (36-nodes elements) and the computations lasted for about 8 seconds, while the solution for the second mesh (441-nodes elements) was not converged unless Δt was chosen as $0.002\,\text{sec}$. The computations time for the second analysis was about 700 seconds (about 11 minutes).

3.2 Wave propagation in an aluminum plate

In the second example, a 2D square aluminum plate is considered to demonstrate the accuracy of SFEM in modeling more realistic structures. Wave propagation in this uncracked plate will be simulated, and then a crack will be embedded in the plate as the third example. The geometry of the isotropic aluminum plate is presented in Figure 7a. The plate

has the following dimensions and material properties: length 1000 mm, width 1000 mm, thickness 1 mm, Young's modulus E = 72.9 GPa, Poisson's ratio v = 0.33, and mass density r = 2700 kg/m^3. Using the mechanical properties of the plate, the primary and secondary wave velocities may be easily calculated as $c_p = 5432.3$ m/s and $c_s = 3144.2$ m/s.

In order to divide the plate into SFEs, a regular structured mesh including 40×40 elements of 36-nodes of 25×25 mm^2 is employed. This SFE mesh has a total number of degrees of freedom (DOFs) equal to 80802. All four edges of the plate are free while its four vertices are constrained in both directions. An excitation signal in the form of a force pulse signal of 100N amplitude has been applied at point A. Figure 8 presents this signal in both time and frequency domains.

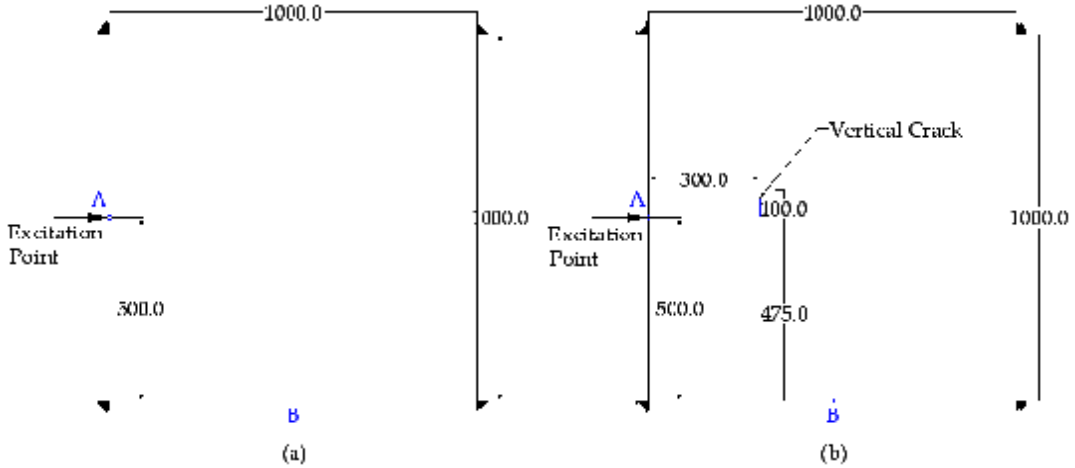

Figure 7. Geometry, loading, and boundary conditions of the aluminum plate of the second and third examples (length unit is in millimeters): (a) uncracked plate, (b) cracked plate

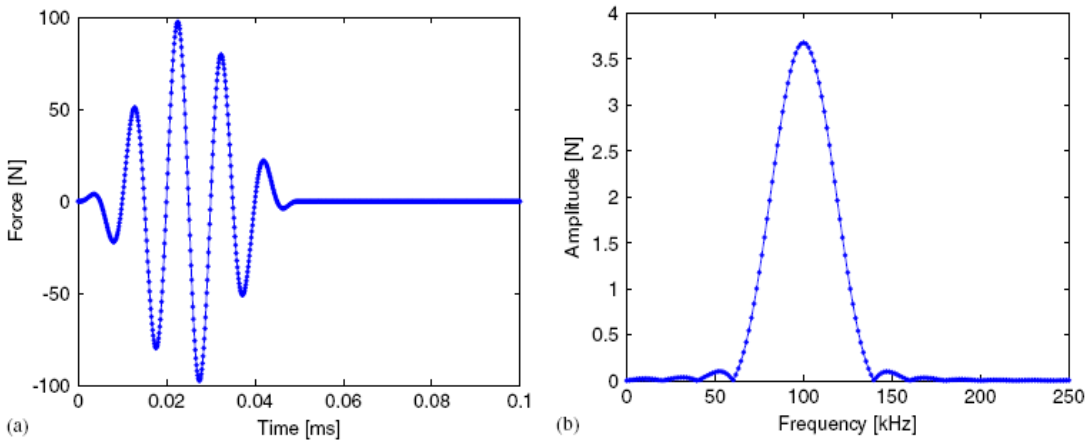

Figure 8. Excitation function applied at point A in (a) time domain and (b) frequency domain

In order to verify the developed SFEM code for 2D problems, the results of SFEM are compared to the results obtained using classical FEM. To this end, various meshes with

different densities are constructed and analyzed using commercial ABAQUS software. These meshes consist of quadrilateral 4-nodes elements whose dimensions are 5×5, 2.5×2.5, 1.667×1.667, and 0.833×0.833 mm^2, respectively. The mentioned meshes involve 80802, 321602, 722402, and 2884802 DOFs, respectively. These DOFs are almost 1, 4, 9, and 36 times of DOFs used in SFEM mesh of the present research.

The results of analyses for both SFEM and classical FEM approaches for horizontal displacements at points A and B (see Figure 7) are drawn in Figure 9. From this figure, one may observe that very fine meshes of FEs give excellent results. In other words, computational costs of classical FEM is by far much more than SFEM while obtaining the same accuracy.

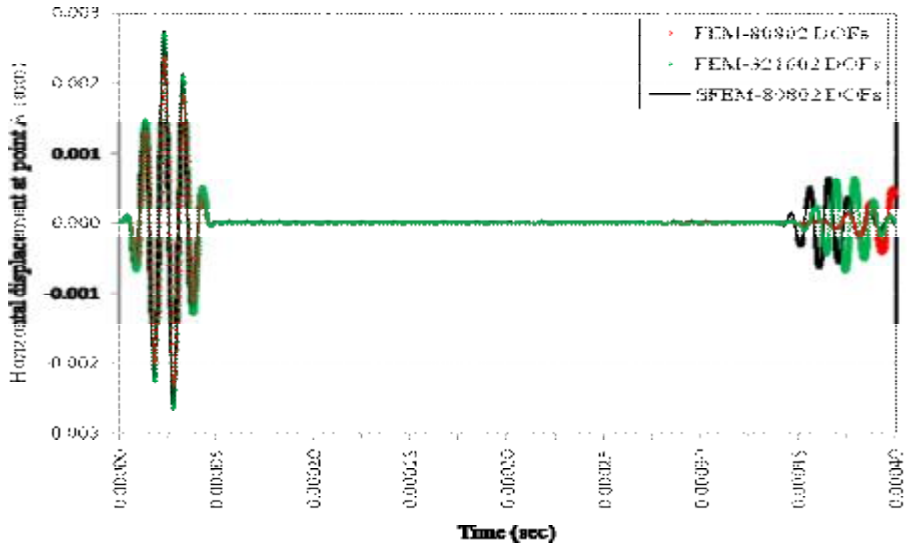

(a)

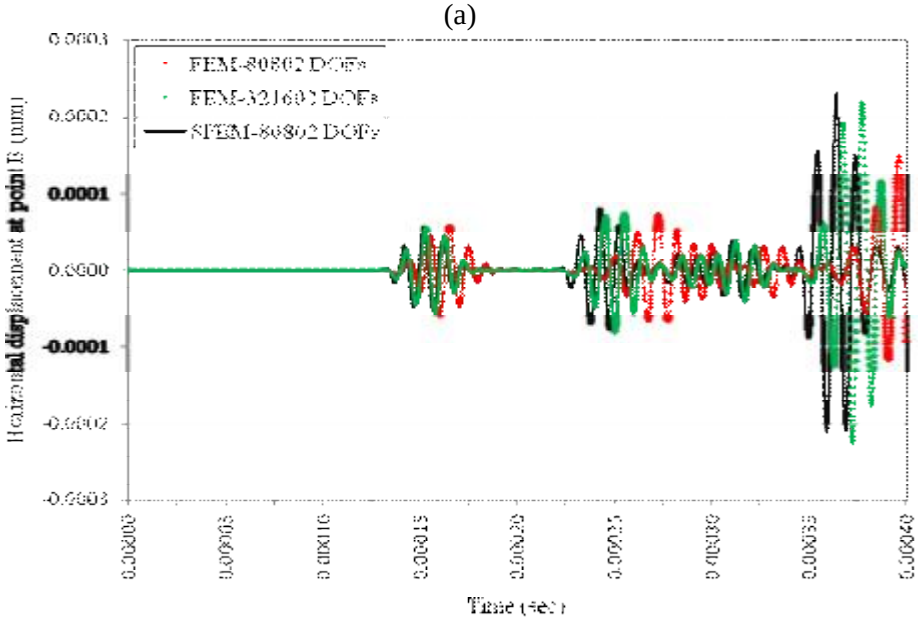

(b)

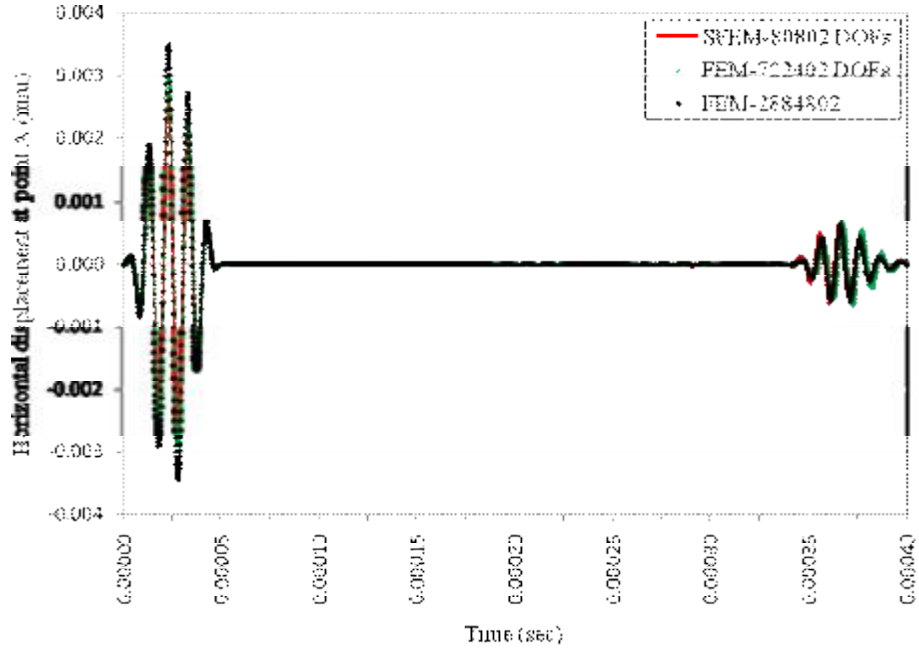

(c)

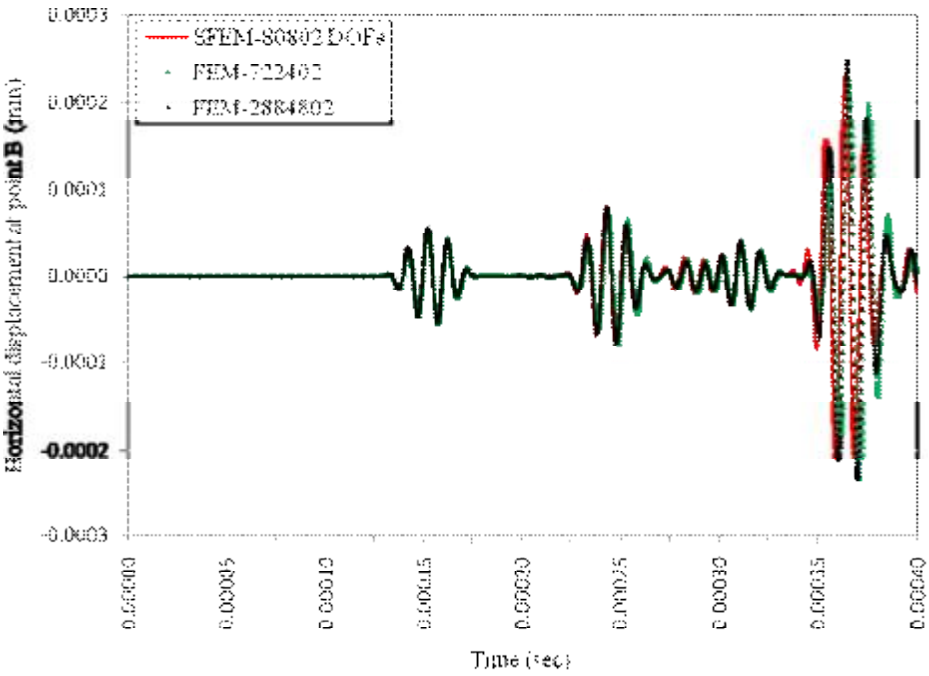

(d)

Figure 9. Horizontal displacements at points A and B obtained by SFEM and classical FEM

In order to show the high-resolution characteristic of obtained results by SFEM, Figure 10 depicts horizontal displacement contours for the entire aluminum plate in nine different time steps, plotted by TECPLOT software.

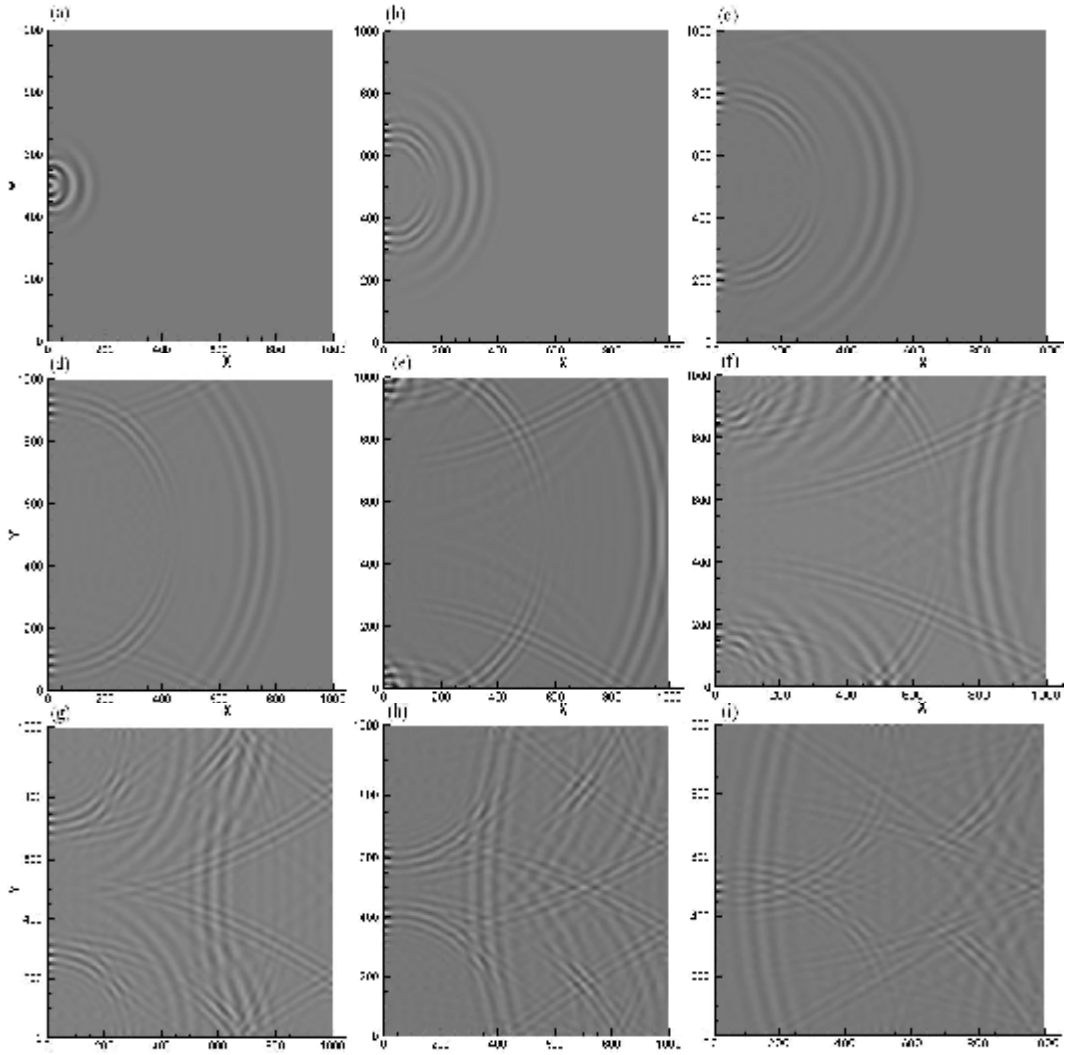

Figure 10. Horizontal displacement contours of aluminum plate plotted in nine different time steps of (a) t = 0.04 ms, (b) t = 0.08 ms, (c) t = 0.12 ms, (d) t = 0.16 ms, (e) t = 0.2 ms, (f) t = 0.24 ms, (g) t = 0.28 ms, (h) t = 0.32 ms, (i) t = 0.36 ms

3.3 Wave scattering in a cracked aluminum plate

In the third and final example, we study the previous plate damaged by a single crack loaded by the same loading, in order to check the accuracy of SFEM in the analysis of wave scattering phenomenon. All assumptions of this example are the same as the previous one. The only difference is that a crack of length 100 mm is located within the plate as shown in Figure 7b. Again, the same parameters have been measured. Similar to preceding example, contours presented in Figure 11 show the wave propagation in the cracked plate. It can be seen that the simulation successfully displays the effect of the crack as could be observed in the form of wave scattering.

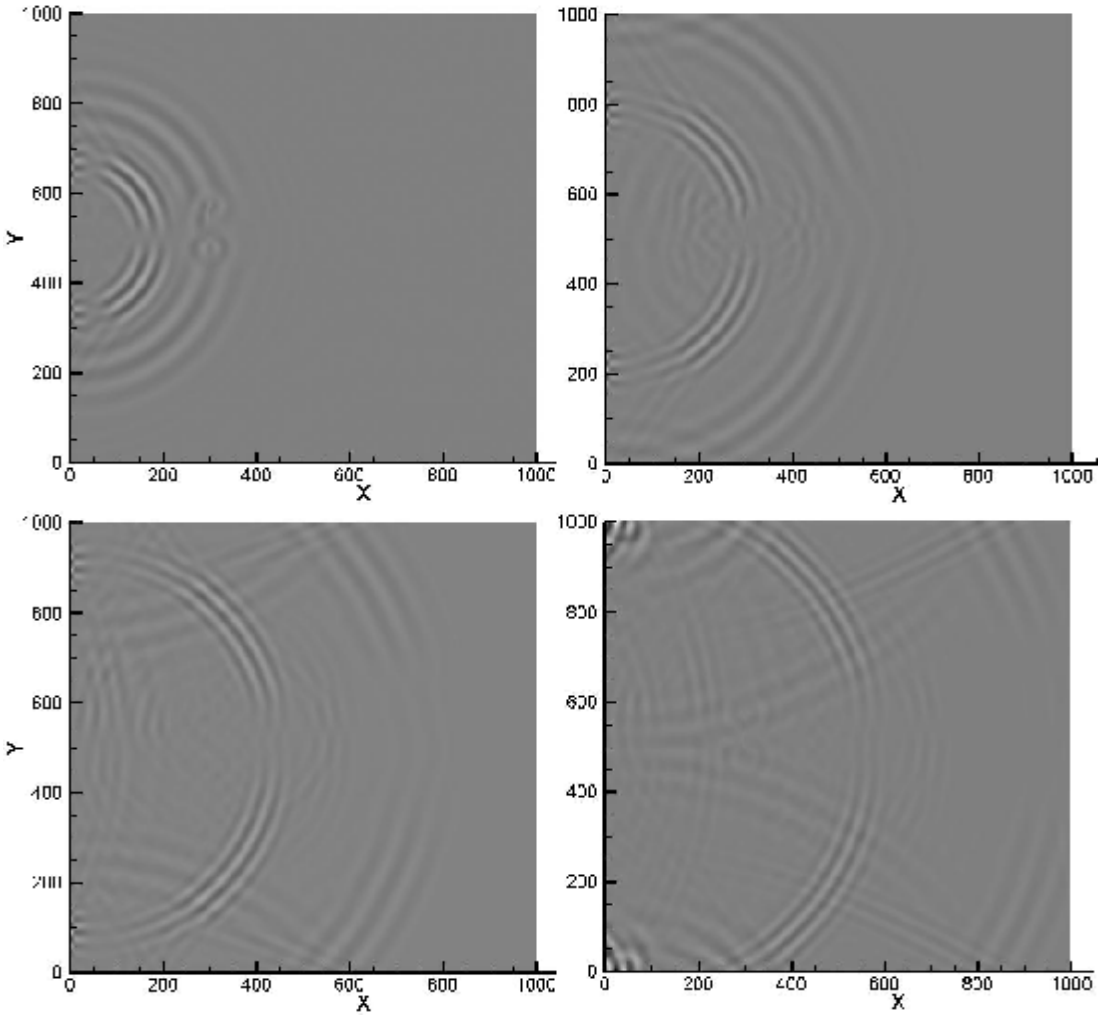

Figure 11. Horizontal displacement contours of cracked aluminum plate plotted in four different time steps

To get better sense on the wave scattering due to the presence of the crack, the time variation of horizontal displacement measured at points A and B in both cases of uncracked (the 2nd example) and cracked (the 3rd example) plates are shown in Figure 12. Although the effect of the presence of the crack might not be clearly visible in Figure 12, however, when the differences of two signals are calculated, the influence of the crack comes out. This differential waveform as a forward solution will be used in a new algorithm to detect an existing crack in the plate as an inverse solution of crack detection problem. See the second part of the present paper for more details.

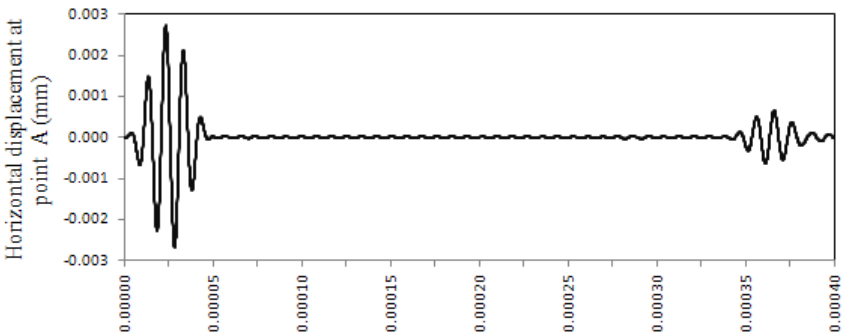

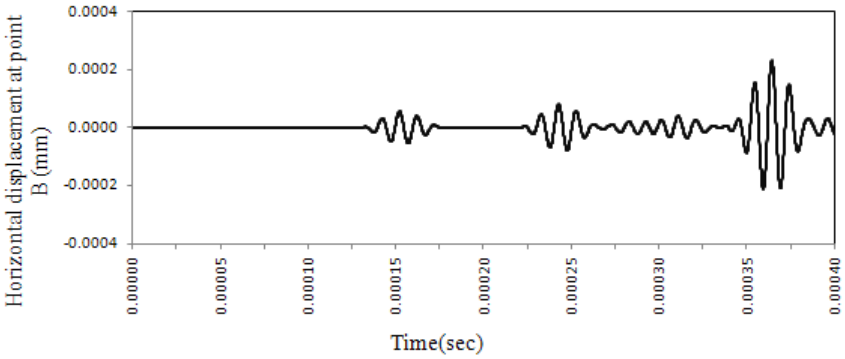

(a)

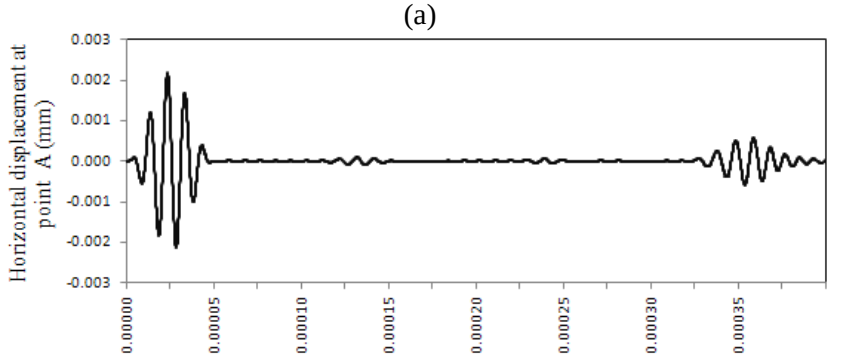

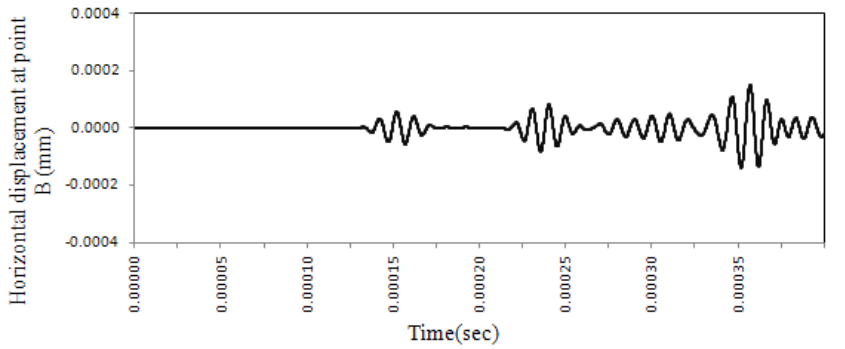

(b)

Figure 12. The time histories of horizontal displacement at points A and B of the aluminum plate for both cases of (a) uncracked and (b) cracked conditions

4. DISCUSSIONS AND CONCLUDING REMARKS

In this paper, detailed introduction of SFEM for modeling transient wave scattering problems in domains made of isotropic materials has been presented. It has been shown that SFEM offers special features over classical FEM which makes it a more powerful and flexible tool dealing with large scale wave propagation problems. Choosing different SFEs, one may obtain different levels of accuracy. Solving the same problem with different SFEs suggests that the precision of solution grows exponentially while increasing the SFEs' order. This exponential increase in precision makes SFEM able to give a converged solution using less DOFs compared to classical FEM. On the other hand it should be noted that when the order of SFEs grows, the minimum length between nodes decreases too, which leads to a smaller critical time increment. Consequently, to make an advance in computational costs (i.e., computation time and memory), an appropriate SFE order should be chosen. This SFE order should establish a balance between spectral convergence rate and spectral critical time increment.

There are some important hints when coding SFEM. Taking these notes into consideration makes a SFEM code faster and much accurate, the first of which is to take the advantage of diagonal mass matrix. The second important point is that if central difference method is used for time integration, there is no need to the global stiffness matrix. Therefore, the formulation of the method could be developed on elemental level which leads to a great machine memory saving.

Transient analyses of three examples have been successfully carried out using the developed code of SFEM. In these examples, various dynamic behaviors, geometries, materials properties, boundary conditions, and transient load functions have been selected to illustrate the applicability and generality of this method. One may note that all examples have been successfully modeled with a few numbers of DOFs, preserving very high accuracy comparing with other analytical and numerical solutions.

As already discussed, considering the applicability and generality of SFEM in wave scattering problems, application of the results of this approach for solving the inverse problem of crack detection problem in plates is presented in the second part of the present paper [29].

REFERENCES

1. Kole JS. Solving seismic wave propagation in elastic media using the matrix exponential approach, *Wave Motion*, **38**(2003) 279–93.
2. Guddati MN, Tassoulas JL. Space-time finite elements for the analysis of transient wave propagation in unbounded layered media, *International Journal of Solids and Structures*, **36**(1999) 4699–723.
3. Al-Khaleefi AM, Ali A, Rajakumar C, Kallivokas LF. Acoustic analysis with absorbing finite elements and far-field computations using free-space Green's functions, *Engineering Analysis with Boundary Elements*, **26**(2002) 929–37.
4. Givoli D, Hagstrom T, Patlashenko I. Finite element formulation with high-order absorbing boundary conditions for time-dependent waves, *Computer Methods in Applied Mechanics and Engineering*, **195**(2006) 3666–90.
5. Boroomand B, Mossaiby F. Dynamic solution of unbounded domains using finite

element method: Discrete Green's functions in frequency domain, *International Journal for Numerical Methods in Engineering*, **67**(2006) 1491–530.
6. Idesman AV. Solution of linear elastodynamics problems with space–time finite elements on structured and unstructured meshes, *Computer Methods in Applied Mechanics and Engineering*, **196**(2007) 1787–815.
7. Carrer JAM, Mansur WJ. Time discontinuous linear traction approximation in time-domain BEM: 2-D elastodynamics, *International Journal for Numerical Methods in Engineering*, **49**(2000) 833–48.
8. Tanaka M, Chen W. Dual reciprocity BEM applied to transient elastodynamic problems with differential quadrature method in time, *Computer Methods in Applied Mechanics and Engineering*, **190**(2001) 2331–47.
9. Chien CC, Chen YH, Chuang CC. Dual reciprocity BEM analysis of 2D transient elastodynamic problems by time-discontinuous Galerkin FEM, *Engineering Analysis with Boundary Elements*, **27**(2003) 611–24.
10. Carrer JAM, Mansur WJ. Alternative time-marching schemes for elastodynamic analysis with the domain boundary element method formulation, *Computational Mechanics*, **34**(2004) 387–99.
11. Soares DJ, Mansur WJ. An efficient stabilized boundary element formulation for 2D time-domain acoustics and elastodynamics, *Computational Mechanics*, **49**(2007) 355–65.
12. Abreu AI, Mansur WJ, Canelas A. Computation of time and space derivatives in a CQM-based BEM formulation, *Engineering Analysis with Boundary Elements*, **33**(2009) 314–21.
13. Soares DJ, Mansur WJ. An efficient time-truncated boundary element formulation applied to the solution of the two-dimensional scalar wave equation, *Engineering Analysis with Boundary Elements*, **33**(2009) 43–53.
14. Hamzeh Javaran S, Khaji N, Moharrami H. A dual reciprocity BEM approach using new Fourier radial basis functions applied to 2D elastodynamic transient analysis, *Engineering Analysis with Boundary Elements*, **35**(2011) 85–95.
15. Hamzeh Javaran S, Khaji N, Noorzad A. First kind Bessel function (J-Bessel) as radial basis function for plane dynamic analysis using dual reciprocity boundary element method, *Acta Mechanica*, **218**(2011) 247–58.
16. Sridhar R, Chakraborty A, Gopalakrishnan S. Wave propagation analysis in anisotropic and inhomogeneous uncracked and cracked structures using pseudospectral finite element method, *International Journal of Solids and Structures*, **43**(2006) 4997–5031.
17. Kirby RM, Sherwin SJ. Stabilisation of spectral/hp element methods through spectral vanishing viscosity: Application to fluid mechanics modelling, *Computer Methods in Applied Mechanics and Engineering*, **195**(2006) 3128–44.
18. Komatitsch D, Vilotte J-P, Vai R, Castillo-Covarrubias JM, Sánchez-Sesma FJ. The spectral element method for elastic wave equations – application to 2-D and 3-D seismic problems, *International Journal for Numerical Methods in Engineering*, **45**(1999) 1139–64.
19. Casadei F, Gabellini E, Fotia G, Maggio F, Quarteroni A. A mortar spectral/finite element method for complex 2D and 3D elastodynamic problems, *Computer Methods in Applied Mechanics and Engineering*, **191**(2002) 5119–48.
20. Khaji N, Habibi M, Mirhashemian P. Modeling transient elastodynamic problems using

spectral element method, *Asian Journal of Civil Engineering*, **10**(2009) 361–80.
21. Mirhashemian P, Khaji N, Shakib H. Soil-structure interaction (SSI) analysis using a hybrid spectral element/finite element (SE/FE) approach. *Journal of Seismology and Earthquake Engineering*, **11**(2009) 83–95.
22. Kudela P, Krawczuk M, Ostachowicz W. Wave propagation modeling in 1D structures using spectral finite elements, *Journal of Sound and Vibration*, **300**(2007) 88–100.
23. Kudela P, Zak A, Krawczuk M, Ostachowicz W. Modeling of wave propagation in composite plates using the time domain spectral element method, *Journal of Sound and Vibration*, **302**(2007) 728–45.
24. Zak A, Krawczuk M, Ostachowicz W. Propagation of in-plane waves in an isotropic panel with a crack, *Finite Elements in Analysis and Design*, **42**(2006) 929–41.
25. Zienkiewicz OC, Taylor RL. *The Finite Element Method*, Butterworth and Heinmann, 5th edition, Oxford, UK, 2000.
26. Timoshenko S, Young DH, Weaver W. *Vibration Problems in Engineering*, John Wiley & Sons, 4th edition, New York, USA, 1974.
27. Chien CC, Wu TY. A particular integral BEM/time-discontinuous FEM methodology for solving 2-D elastodynamic problems, *International Journal of Solids and Structures*, **38**(2001) 289–306.
28. Yu G, Mansur WJ, Carrer JAM, Lie ST. A more stable scheme for BEM/FEM coupling applied to two-dimensional elastodynamics, *Computers and Structures*, **79**(2001) 811–23.
29. Kazemi Noureini H, Khaji N. Detection of a through-thickness crack based on elastic wave scattering in plates, Part II: Inverse Solution, *Asian Journal of Civil Engineering*, No. 4, 13(2012), in press.